Nonlinear optical response of highly energetic excitons in GaAs: Microscopic electrodynamics at semiconductor interfaces

M. Betz, G. Göger, and A. Leitenstorfer
Physik-Department E 11, Technische Universität München, D-85748 Garching, Germany

M. Bichler and G. Abstreiter
Walter-Schottky-Institut, Technische Universität München, D-85748 Garching, Germany

W. Wegscheider
Institut für Angewandte und Experimentelle Physik, Universität Regensburg, D-93040 Regensburg, Germany

A spectroscopic investigation of bound electron-hole pairs in GaAs propagating with large center-of-mass momentum is presented. The approach is based on transmission experiments exploiting the coupling of excitonic polarization to the electromagnetic field of femtosecond laser pulses. The dispersion relations of the coherent excitations are determined up to excess energies of 300 meV above the band edge. A surprisingly low Fröhlich coupling of light-hole excitons is observed in excellent agreement with theoretical simulations. The influence of different phonon scattering processes on the excitonic damping is discussed. The interaction dynamics of excitonic wave packets with nonthermal carrier distributions is analyzed with femtosecond time resolution. A theoretical model based on the exciton-polariton concept including additional boundary conditions reproduces our experimental results. The observations in extremely thin samples show deviations from our phenomenological model. This finding is important for a detailed understanding of the microscopic polarizability near semiconductor surfaces.

I. INTRODUCTION

Optical spectroscopy of electronic excitations in direct-gap semiconductors is a central topic in solid-state physics. Many diverse aspects such as electronic band structure, plasmons and single-particle spectra have been elucidated by linear experiments. With the development of ultrashort laser sources, fundamental new questions on nonequilibrium properties of semiconductors have become accessible.[1] Numerous investigations have been devoted to the properties of excitons with negligible kinetic energy in both bulk material and modulated nanostructures.[2] Experimental and theoretical publications have provided a detailed understanding of the dynamical properties of excitons and the interaction processes of these quasiparticles with free carriers and phonons.

Much less is known about the properties of excitons with large center-of-mass velocity. These excitations are usually considered to be inaccessible by optical spectroscopy: first-order interband transitions in crystalline solids occur almost vertically in the band structure since the wave vector of the incident electromagnetic radiation is negligible as compared to the reciprocal lattice vector. Therefore, absorption of photons with energies in the absorption continuum of direct semiconductors is expected to result exclusively in the generation of unbound electron-hole pairs.

Closely related to the question of large-momentum excitons is the polariton concept describing the interplay of a propagating light field with the excitonic polarization.[3] Polaritons have been investigated extensively in experiments focusing on the frequency regime close to the fundamental resonance near the band edge.[4–9] The problem of light propagation through samples with surfaces presents considerable theoretical difficulties because the polarization exchanges momentum with the electromagnetic field.[10–14] Therefore, the semiconductor response deviates strongly from an infinitely extended medium. In the last few years there has been a renewed debate about the correct description of polariton propagation in realistic sample configurations.

In this paper, investigations on large-momentum excitons in GaAs are presented. The experiment relies on highly sensitive femtosecond transmission measurements of thin GaAs films. Preliminary results in this field have been published recently.[15] The present paper contains additional experimental findings and numerical calculations based on a realistic model. It comprises a more detailed discussion and is organized as follows: after the Introduction, Sec. II describes the exciton-polariton concept underlying the interpretation of our data. Section III introduces the experimental technique and discusses essential issues of the sample properties. In Sec. IV, experimental results and numerical calculations of exciton-phonon scattering are presented. Especially, we demonstrate polariton effects in thin layers of GaAs at room temperature. This finding might open up applications in nonlinear optical devices. Section V concentrates on dynamical aspects of the exciton-carrier interaction. For the first time, the excitonic damping is directly measured as a function of the photocreated carrier density. Surprisingly, we find the scattering of large-momentum excitons with nonthermal carriers to be drastically reduced with respect to the fundamental resonance. This result is tentatively explained by phase-space arguments in combination with the nature of the Coulomb matrix element. Moreover, a low density limit of $N \approx 10^{14}$ cm^{-3} is derived where the dynamics is no longer influenced by Coulomb scattering. A theoretical model refin-

ing the considerations in our earlier work[15] is developed in Sec. VI. Especially, we now include all relevant exciton-phonon interaction processes and the dissociation into continuum states in our simulation. These results elucidate the striking difference of the damping of heavy-hole and light-hole excitons. Moreover, a critical assessment of different additional boundary conditions is given. A model modifying Pekar's approach is found to fit best to the experimental observations. Specific phenomena arising for extremely thin semiconductor layers are discussed in Sec. VII. For a slab thickness approaching the excitonic Bohr radius we find a dominant role of interface properties. Interestingly, direct evidence for modifications of the excitonic wave function at the semiconductor interface due to Coulomb screening is found. Finally, a summary is given in Sec. VIII.

II. EXCITON-POLARITON CONCEPT

The description of the optical properties of weakly damped excitons in direct-gap semiconductors is distinctly different from the case of free electron-hole pairs with dephasing times of the order of 100 fs.[16,17] The coherent interaction between the incident electromagnetic wave and the excitonic polarization induced in the sample leads to the formation of new quasiparticles called exciton polaritons. Neglecting scattering events, these polarization waves are coherently reconverted to photons at the exit surface of the medium. Absorption occurs only if polaritons suffer collisions, e.g., with phonons.

In principle, the calculation of the dispersion relation of exciton polaritons is quite difficult for realistic sample geometries, e.g., for a thin slab of the semiconductor material. On the other hand, it is well established that most of the properties may be discussed in terms of the solution of the polariton problem for a homogeneous, infinitely extended medium (for a detailed description, see e.g., Ref. 2). For our experiments in GaAs three charge carriers are relevant: conduction electrons, heavy holes (hh), and light holes (lh) with effective masses m_e, m_{hh}, and m_{lh}, respectively. Since the oscillator strength of higher bound states turns out to be small, polariton phenomena are considered for $1s$ excitons only.[18] In parabolic approximation, the dispersion relation is determined by the implicit equation

$$\hbar^2 c^2 K^2 / E^2 = \varepsilon(E,K)$$

$$= \varepsilon_{st}\left(1 - \sum_{j=hh,lh} \frac{E_{LT,j}}{E - E_j - \hbar^2 K^2 / 2M_j + i\Gamma_j}\right), \quad (1)$$

where ε_{st} is the static dielectric constant and $M_j = m_j + m_e$ are the effective masses of the excitons ($j = $ hh, lh). The energetic positions of the fundamental exciton resonances are denoted as E_j and their damping with Γ_j. Near E_j zero crossings of the dielectric function $\varepsilon(E,K)$ are found allowing longitudinal polariton modes. The difference $E_{LT,j}$ of their energetic position and the exciton energy E_j is proportional to the oscillator strength of the excitonic transition. In GaAs, these values are $E_{LT,hh} = 0.08$ meV and $E_{LT,lh} = \frac{1}{3}E_{LT,hh}$ due to the smaller transition matrix element for lh
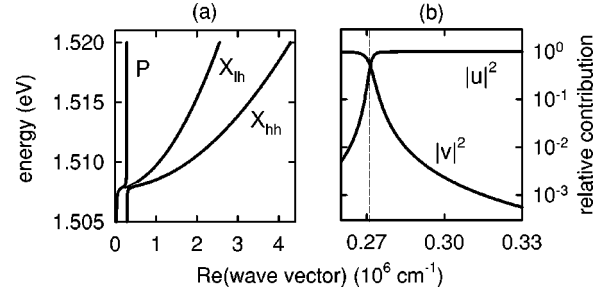

FIG. 1. (a) Three bands of the polariton dispersion in GaAs calculated with effective exciton masses $M_{hh} = 0.52\ m_0$, $M_{lh} = 0.19\ m_0$. (b) Excitonic ($|u|^2$) and photonic ($|v|^2$) contributions calculated for the polariton branch X_{hh}. Note the different scale of the abscissa.

excitons.[19] Band mixing is not included in our discussion of hot excitons since this effect is only relevant very close to the band edge.

Figure 1(a) displays the three polariton bands calculated with Eq. (1) in the limit of low damping. Only a few meV above the fundamental exciton at 1.508 eV the polariton modes have perfectly recovered their unperturbed dispersion: the spectrum contains a linear photonlike mode (P) with very steep slope and two parabolic excitonlike branches with effective masses of heavy-(X_{hh}) and light-hole (X_{lh}) excitons. Accordingly, the mixing of photonic and excitonic contributions[20] to the hh excitonlike polaritons X_{hh} is only relevant in the vicinity of the crossing of the unperturbed dispersions [see Fig. 1(b)]: for smaller wave vectors the hh polariton wave function contains almost exclusively photonic contributions ($|(v)|^2 \approx 1$), while above the crossing the photonic admixture $|(v)|^2$ decreases rapidly to values below 10^{-3} corresponding to excitonlike quasiparticles ($|(u)|^2 \approx 1$). For increasing dephasing rates of the excitons the mixing of photonic and excitonic components decreases. Above a critical damping $\Gamma_{\mathrm{crit},j} = (8E_{LT,j}E_j^2\varepsilon_{\mathrm{st}}/M_jc^2)^{1/2}$ (Ref. 20), which has a value of 0.26 meV for both hh and lh excitons in GaAs the anticrossing disappears and polariton phenomena are no longer relevant.

III. EXPERIMENTAL TECHNIQUE

A. Samples

Our measurements are performed on molecular-beam-epitaxy-grown, ⟨100⟩-oriented, very high-purity GaAs films with thicknesses of 50 nm, 200 nm, and 500 nm. They are clad by an $Al_{0.3}Ga_{0.7}As$ layer on one side. Excitonic line widths below 1 meV indicate high quality growth and long intrinsic dephasing times of the fundamental exciton. For our transmission experiments, the GaAs substrate was etched away. The samples are antireflection coated on both sides with Si_3N_4 and mounted on sapphire substrates via van der Waals bonding. They are held inside a closed-cycle cryostat to assure low lattice temperatures of $T_L = 20$ K.

It is important to emphasize that a very high quality sample is necessary to observe unambiguous spectra. The semiconductor specimen has to have a high homogeneity over the lateral measuring range (i.e., diameter between 100 μm

and 500 μm). If the thickness variation Δd of the GaAs specimen exceeds a few nm across the probing area, the observation of the interference phenomena reported in this paper is not possible. The reason for this extreme requirement on the surface quality of the samples is the large wave vector K of the investigated quasiparticles. Even for highly energetic heavy-hole excitons with wave vectors of the order of 1×10^7 cm^{-1} the condition $K\Delta d \ll 1$ has to be fulfilled to obtain reliable results.

B. Experimental setup

Our experiments are based on femtosecond transmission experiments using a special two-color femtosecond Ti:sapphire laser.[21] The system provides two independently tunable pulse trains with durations from 13 fs to 120 fs at a pulse repetition rate of 76 MHz. The accessible photon energies range from 1.45 eV to 1.77 eV, well matched to the band-gap energy $E_G = 1.51$ eV of GaAs at temperatures of $T_L = 20$ K. The more intense branch of the laser is tuned to photon energies high up in the absorption continuum of GaAs. This pump pulse of 100 fs duration excites the sample over a lateral diameter of typically 1 mm and produces a density of free electron-hole pairs up to 6×10^{16} cm^{-3}. The second branch of the laser output serves as an ultrashort broadband probe continuum. It encompasses the entire spectral range from below the $1s$ exciton to about 300 meV above the band edge. The excitation density of the probe pulse is held around 10^{14} free electron-hole pairs per cm^3 in order to suppress disturbing influences of probe-created nonthermal carriers (see Sec. V B for a discussion of results depending on the probe generated carrier density). The temporal separation of the two pulse trains is adjusted via a variable delay line. The probe pulse train passes the central part of the excitation spot on the sample in order to investigate an area of homogeneuous carrier density. After transmission through the sample the probe spectrum is dispersed in a double monochromator with a resolution of 0.6 meV and detected with a standard silicon photodiode. Lock-in amplification operating at 10 kHz enables us to measure pump-induced transmission changes below 1×10^{-6}, limited only by the shot-noise of the probe photon current.

IV. EXCITON-PHONON SCATTERING

A. Experimental results for different layer thicknesses

Pump-induced transmission changes versus probe photon energy in GaAs specimens with 50 nm, 200 nm and 500 nm thickness are displayed in Fig. 2. The spectra are recorded 10 ps after excitation of unbound electron-hole pairs with the pump pulse. This delay time is chosen to investigate a quasistatic situation and to avoid underlying bleaching effects due to highly energetic electrons.[16,17,25] The transmission changes observed in the 500-nm sample [see Fig. 2(a)] around the fundamental exciton resonance at 1.509 eV are large and well understood as the nonlinear optical response of the fundamental exciton polariton: slight strain in the sample removes the degeneracy at the top of the valence bands and leads to two peaks for hh and lh excitons at 1.508
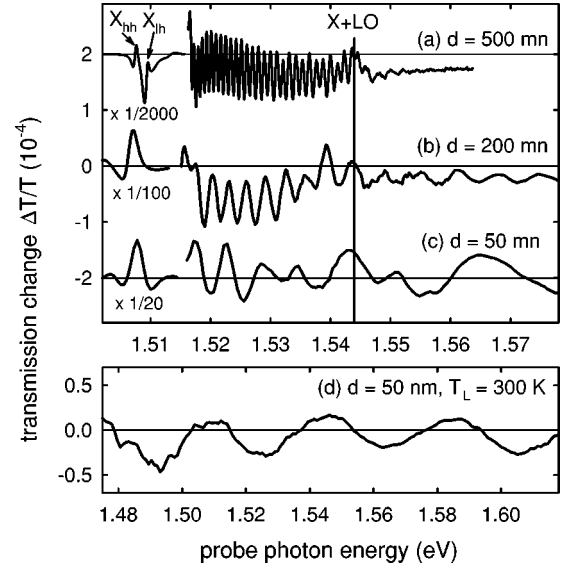

FIG. 2. Spectrally resolved transmission changes as measured 10 ps after injection of unbound electron-hole pairs in GaAs layers with (a) 500 nm, (b) 200 nm, and (c) 50 nm for a lattice temperature of $T_L = 20$ K. The pump generated carrier densities are (a) $N = 3 \times 10^{15}$ cm^{-3}, (b) 5×10^{15} cm^{-3}, and (c) 3×10^{16} cm^{-3}. (d) Differential transmission spectrum recorded in the 50-nm specimen 10 ps after injecting 6×10^{16} cm^{-3} free carriers at room temperature.

eV (X_{hh}) and 1.510 eV (X_{lh}), respectively. Simultaneous broadening of the excitonic transitions and increasing total absorption induced by the pump generated carriers results in the observed spectral shape: induced absorption with a local bleaching peak centered in the middle of the exciton line.[6]

In the absorption continuum above 1.515 eV well-resolved propagation beats appear in the differential spectra. This phenomenon may be understood via the picture outlined in Sec. II: When probe photons corresponding to the absorption continuum are incident on the sample surface, three propagating modes (P, X_{hh}, and X_{lh}, see Fig. 1) are accessible inside the medium. Due to the break of translational symmetry at the semiconductor interface, momentum conservation is not strictly valid. As a consequence, small fractions of the incident radiation also excite excitonlike polaritons. These quasiparticles propagate through the sample with a typical group velocity of the order of 1×10^7 cm/s as determined by the parabolic center-of-mass dispersion of hh and lh excitons. The three polarization components travel through the semiconductor layer and are coherently reconverted to photons at the exit surface. The additional electric-field amplitudes resulting from the polarization of the excitonlike polaritons result in tiny interference patterns on the transmitted spectrum reflecting the different phase velocities of the three polariton modes.

A different situation is found after excitation of a excess carrier distribution generated by the pump pulse. Now the dephasing of the excitons is increased due to the efficient exciton-free carrier scattering. Therefore, only the photonlike polaritons are transmitted through the sample while the modes with high admixture of excitonic polarization are damped out before reaching the exit surface of the semicon-

ductor. Since our photomodulation technique measures the difference of the transmitted spectra with and without excitation, the large background of probe photons propagating on the photonlike mode is substracted and the differential spectra are dominated by contributions of the excitonlike polaritons.

Assuming a parabolic band structure with an effective exciton mass M_X, the energetic period ΔE of the resulting propagation beats in a semiconductor layer with thickness d is determined by

$$\Delta E = \frac{2\pi\hbar \sqrt{2E_{\text{kin}}/M_X}}{d}. \qquad (2)$$

Considering this relation two beating modes can be identified in the differential spectrum of the 500-nm specimen [see Fig. 2(a)]. The fast beating component corresponds to the 1s hh exciton. Above a kinetic energy of one LO phonon energy of $\hbar\omega_{LO} = 36$ meV this component is strongly damped due to polar optical scattering (see Sec. IV B). Slower oscillations originating from lh excitons can be seen even above this threshold energy. The interference pattern may be exploited to fit effective exciton masses according to Eq. (2). Values of 0.52 m_0 and 0.19 m_0 are found in the $\langle 100 \rangle$-direction reproducing the hh-lh beating structure near $X+$LO. The experimental result for hh excitons is consistent with the sum of the band-edge effective masses of electrons and heavy holes in $\langle 100 \rangle$ direction.[22] The observed effective mass of light holes of $m_{lh}^{\langle 100 \rangle} \approx 0.12$ m_0 is significantly larger than the value of $m_{lh} = 0.082$ m_0 found in cyclotron resonance experiments.[22] This effect indicates a higher nonparabolicity of the lh band that is relevant already for exciton energies around 1.54 eV.[23]

In the 200-nm specimen [see Fig. 2(b) and Fig. 10(a)] the polariton beating is observed up to 300 meV above the band edge. Again, both hh and lh components contribute to the observed oscillation for photon energies below $X+$LO. Above the threshold for emission of LO phonons only oscillations associated with lh excitons are found. Apparently the Fröhlich coupling of these quasiparticles is surprisingly low to allow propagation of lh excitons over distances of 200 nm without strong damping due to LO phonon emission. The oscillation period remains approximately constant for transition energies above 1.58 eV indicating a linear lh exciton dispersion in this regime.

In the 50-nm GaAs layer [see Fig. 2(c)] polariton interference effects are also observed for excess energies as large as 200 meV above the band edge. A closer analysis of the spectra obtained with this sample is given in Sec. VII. Surprisingly, polariton interference effects in the 50-nm specimen are visible even at room temperature $T_L = 300$ K [see Fig. 2(d)]. This finding demonstrates that coherent propagation of highly energetic excitons remains relevant for elevated temperatures where excitonic effects are usually believed to be of minor importance in bulk GaAs.

B. Polariton-LO phonon scattering

The interaction of bound electron-hole pairs with optical and acoustic phonons is calculated analogous to the scatter-

ing of free charge carriers. The matrix element for an exciton scattering from a state $|n, \mathbf{K}\rangle$ to a state $|n', \mathbf{K}+\mathbf{q}\rangle$ (with n, n' describing the internal motion of the exciton and $\mathbf{K}$, $\mathbf{K}+\mathbf{q}$ denoting the center-of-mass wave vector of the exciton) is given by the sum of electron and hole contributions weighted with form factors S:[20,24]

$$I_{n,\mathbf{K}}^{n',\mathbf{K}+\mathbf{q}}(\mathbf{q}) = C_{\mathbf{q},\text{e}} S_n^{n'}(p_{\text{e}}\mathbf{q}) - C_{\mathbf{q},\text{h}} S_n^{n'}(-p_{\text{h}}\mathbf{q}), \qquad (3)$$

$$S_n^{n'}(\mathbf{q}) = \int d\mathbf{r} \Phi_{n'}^*(\mathbf{r}) e^{i\mathbf{q}\mathbf{r}} \Phi_n(\mathbf{r}). \qquad (4)$$

In these equations $p_{\text{e}} = m_{\text{h}}/(m_{\text{h}}+m_{\text{e}})$ and $p_{\text{h}} = (m_{\text{e}}/(m_{\text{h}}+m_{\text{e}})$ are determined by the effective masses m_e and m_h of the charge carriers. The coupling constants $C_{\mathbf{q},e}$ and $C_{\mathbf{q},h}$ denote the interaction strength for electrons and holes with a phonon with wave vector $\mathbf{q}$. $\Phi_n(\mathbf{r})$ is the part of the excitonic wave function reflecting the relative motion of the charge carriers (e.g., $\Phi_1(\mathbf{r}) = e^{-r/a_B}/\sqrt{\pi a_B^3}$ for the case of 1s excitons with Bohr radius a_B). The interference of electron-phonon and hole-phonon interaction [note the different signs of the two contributions in Eq. (3)] is especially important for the case of polar optical scattering where the coupling constant is identical for both types of charge carriers,[26]

$$C_q^2 = \frac{\hbar e^2 \omega_{LO}}{2\varepsilon_0 V} \left(\frac{1}{\varepsilon_\infty} - \frac{1}{\varepsilon_{st}} \right) \frac{1}{\mathbf{q}^2}. \qquad (5)$$

The Fourier transform $S_n^n(p_{\text{e (h)}}\mathbf{q})$ of the charge carrier distribution of the electron (hole) describes the internal motion in the exciton and determines the effectiveness of the coupling to a phonon with wave vector $\mathbf{q}$. For the case of scattering within the 1s exciton band this factor is given by

$$S_{1s}^{1s}(\mathbf{q}) = \frac{1}{[1+(\mathbf{q}a_B/2)^2]^2}. \qquad (6)$$

As may be seen from the structure of the form factors, the scattering process is dominated by phonons with wave vectors in the order of the reciprocal Bohr radius. Scattering to higher bound states of the exciton is less effective due to the decreasing overlap of the envelope functions in Eq. (4). For kinetic energies above $\hbar\omega_{LO}$ the fastest relaxation process is—as for the case of free charge carriers—the polar optical emission of LO phonons.

Figure 3(a) shows the calculated Fröhlich scattering rates for 1s hh excitons in GaAs for a lattice temperature of $T_L = 20$ K. Scattering within the 1s exciton dispersion exhibits a rate of 5 ps^{-1} and is approximately as fast as the LO phonon emission of hot electrons in GaAs.[16,17,25] Scattering into 2p or 2s (not shown in Fig. 3) hh states is slow as compared to intraband scattering. It should be noted that scattering into lh excitons is calculated to be substantially weaker than intraband relaxation. The dissociation into continuum states begins to dominate for kinetic energies above 60 meV. The absorption of LO phonons is calculated to be negligible in this temperature regime [see also Fig. 5(b)]. As displayed in Fig. 3(b), the polar optical intraband scattering is dominated by the hole contribution in Eq. (3).
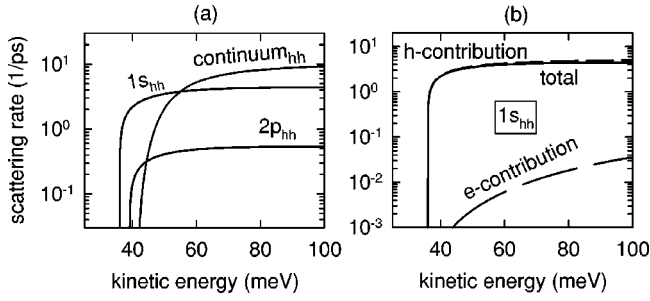
FIG. 3. (a) Calculated polar optical scattering rates of $1s$ hh excitons in GaAs into the states $1s_{hh}$, $2p_{hh}$ and into continuum states for a lattice temperature of $T_L = 20$ K. (b) Electron and hole contribution to the intraband scattering rate of $1s$ hh excitons.

Considering these scattering rates of hh excitons, the discontinuity of the interference spectra at the energetic position $X + LO$ [see Figs. 2(a) and (b)] is readily understood: the mean free path of hh excitons above the threshold for emission of LO phonons is 20 nm to 30 nm and therefore small as compared to the propagation distances in the samples with 200 nm or 500 nm thickness.

A completely different situation is found in the calculated scattering rates for lh excitons in GaAs (see Fig. 4). Due to the fact that lh excitons consist of quasiparticles with similar effective masses and the coupling constant $C_{\mathbf{q}}$ of electrons and holes is the same for polar optical interactions [see Eq. (5)], destructive interference effects between electron and hole contributions in Eq. (3) become important. The physical reason for this effect is the reduction of the polar optical interaction energy with the macroscopic polarization field of LO phonons for the case of similar spatial charge distributions of electron and hole.
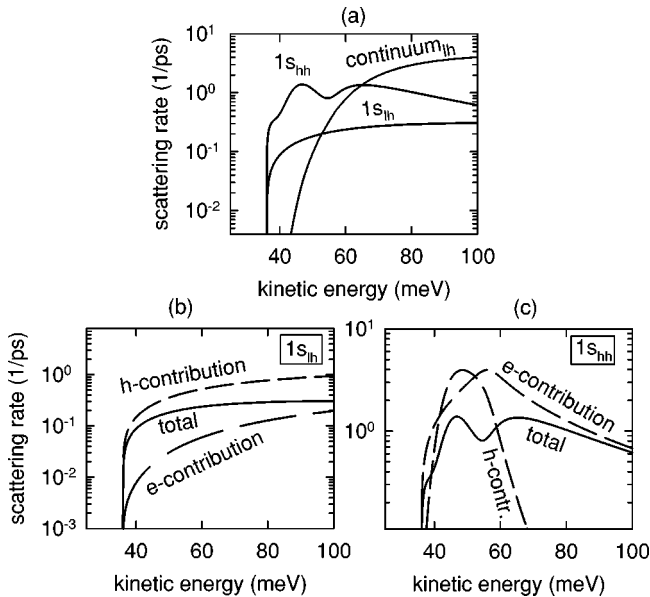

FIG. 4. (a) Calculated polar optical scattering rates of 1s lh excitons in GaAs into the states $1s_{lh}$, into unbound electron-hole pairs and into $1s$ hh excitons for a lattice temperature of $T_L = 20$ K. (b) and (c) Electron and hole contributions for the polar optical scattering within the $1s$ lh exciton dispersion and into $1s$ hh excitons.
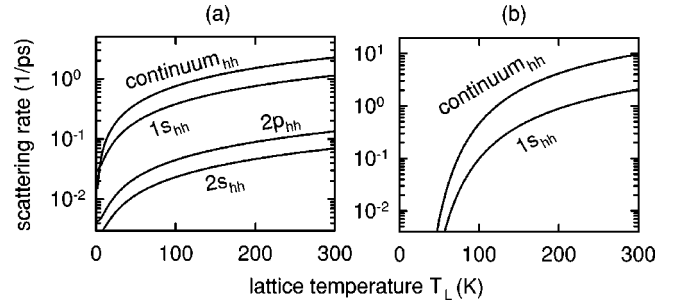

FIG. 5. Calculated scattering rates for hh excitons with a kinetic energy of 25 meV as a function of temperature: (a) acoustic deformation potential scattering into $1s_{hh}$, $2s_{hh}$, $2p_{hh}$ excitons and into continuum states. (b) Corresponding simulations for absorption of LO phonons via the polar optical mechanism.

As may be seen from Fig. 4(a), the scattering of lh excitons is drastically reduced with respect to hh excitons (scattering to higher bound states of the lh exciton dispersion is found to be negligible and is omitted for clarity). Figures 4(b) and 4(c) show the drastic consequences of the interference effect. Although light holes relax extremely fast via polar optical scattering,[27,28] this process is strongly slowed down for lh excitons. The scattering time of 700 fs for lh excitons with a kinetic energy of 55 meV is a factor of 20 longer than the calculated interband scattering time of light holes. Interestingly, the reduction of the scattering rates is observed for both interband and intraband transitions: the relaxation time of lh excitons into hh states is reduced by a factor of 20 with respect to polar optical scattering of free light holes. These time scales explain the surprising observation of lh excitons propagating over a sample thickness of 200 nm up to kinetic energies large as compared to the LO phonon energy. Again, for kinetic energies above 60 meV, the relaxation is dominated by scattering into continuum states. Surprisingly, the modified overlap integral reduces the dissociation rate by a factor of 3 as compared to hh excitons even for the dissociation channel.

C. Polariton-acoustic phonon scattering

The polariton interference spectra were also studied as a function of temperature. The results recorded with the 500-nm sample at a delay time of $t_D = 10$ ps are displayed in Fig. 4 of Ref. 15. The observed oscillation amplitude decreases with increasing temperature. Above $T_L = 100$ K the propagation beats vanish due to efficient damping of the excitons. In order to understand the physical origin of this damping, numerical simulations are performed for the damping of hh excitons below the threshold for LO phonon emission.

Figure 5(a) displays the damping of hh excitons with a kinetic energy below $\hbar \omega_{LO}$ via acoustic deformation potential scattering. The coupling strength for this interaction is given by[26]

$$C_q^2 = \frac{\hbar}{\rho v_S V} D_s^2 q, \tag{7}$$

where ρ and v_S are the mass density and the sound velocity of GaAs. The acoustic deformation potentials averaged over the directions in k space are $D_h = 5.6$ eV for holes and $D_e = -3.4$ eV for electrons in GaAs.[28]

For comparison, the corresponding polar optical scattering times due to absorption of LO phonons are depicted in Fig. 5(b). Piezoelectric scattering is calculated to be negligible as compared to the dominant processes in Fig. 5(a).

For temperatures up to 120 K, acoustic deformation potential scattering is the fastest dephasing mechanism for large-momentum excitons below the LO phonon threshold. This finding is consistent with experimental results for the fundamental exciton resonance in quantum wells.[30] For a temperature of 100 K the sum of the calculated relaxation channels leads to a total damping of 1.5 ps^{-1}. Comparing this value to a propagation time of 4 ps for hh excitons with 25-meV kinetic energy through the 500-nm specimen, the temperature-dependent oscillation amplitude is consistent with our calculations. Surprisingly, the damping of large-momentum excitons via acoustic phonons does not differ strongly from the fundamental exciton resonance. The excitonic damping due to acoustic phonons may be characterized by a coefficient σ for the increase of the homogeneous linewidth with temperature: from both experiment and temperature-dependent calculations $\sigma = 20$ μeV/K is estimated. This result is close to the corresponding value of $\sigma = 17$ μeV/K for the fundamental exciton resonance.[29]

V. EXCITON-FREE CARRIER SCATTERING

In the preceding section, the results have focused on quasistatic aspects of exciton-polariton phenomena. On the other hand, our technique employing ultrashort laser pulses opens up the possibility to study the dephasing dynamics of large wave vector excitons with femtosecond time resolution where interaction with hot charge carriers occurs. Extending our previous work,[15] the scattering time for large-momentum excitons with a nonthermal electron-hole plasma is directly measured for different carrier densities. The damping is shown to be drastically reduced with respect to the fundamental exciton resonance. By varying the intensity of the probe beam, a low density limit of $N = 10^{14}$ cm^{-3} is observed, where the dynamics is no longer influenced by Coulomb scattering.

A. Experimental results for time resolved polariton propagation

Differential transmission spectra obtained in the 500-nm layer are recorded as a function of the temporal separation of the exciting and probing laser pulses (see Fig. 6). For negative delay times t_D the arrival of the probe pulse precedes the injection of free carriers via the pump pulse. Therefore, the excitonic wave packets suffer enhanced excitation-induced damping only for part of their propagation through the layer. As a consequence, the time-dependent polariton interferences reflect the damping dynamics of the large-momentum excitons.

The results in Fig. 6 may be understood as follows: the interference pattern for the time interval -3.5 ps$\lesssim t_D$
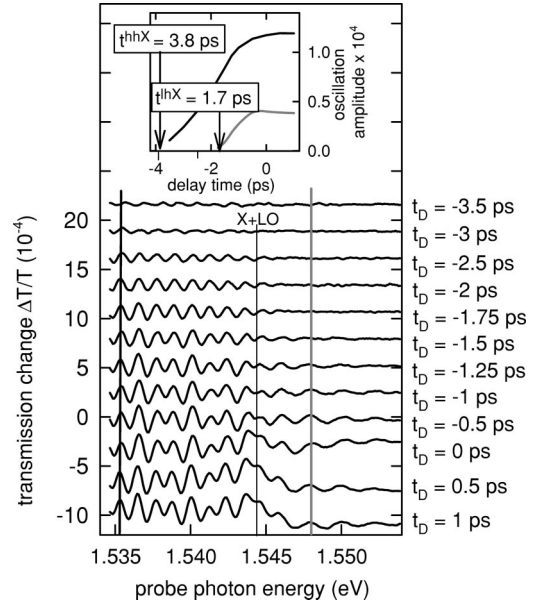

FIG. 6. Differential transmission spectra of the 500-nm GaAs layer near probe photon energies of $X + LO = 1.544$ eV for different delay times t_D. Experimental parameters are chosen as in Fig. 2(a). Inset: amplitude of the spectral oscillation versus t_D at probe photon energies of 1.536 eV and 1.548 eV as indicated by the vertical lines.

$\lesssim -2$ ps contains only a fast beating component with an abrupt discontinuity near $X + LO$. These propagation beats correspond to hh excitons, while lh excitons exhibit propagation times below 2 ps through the 500-nm layer due to their small effective mass and large group velocity. For the case of $t_D > -1.5$ ps slower oscillations are observed above the threshold energy $X + LO$: these beats reflect the damping dynamics of lh excitons. For delay times $t_D \gtrsim 0$ both branches suffer efficient damping along the entire crystal thickness and an underlying bleaching effect due to the pump generated nonthermal charge carriers is observed.[16,17,25]

To get a physical picture of the time-dependent oscillation amplitude, we consider a phenomenological model: the injection of unbound nonthermal carriers enlarges the initial dephasing rate Γ_0 of the excitonic wave packet to $\Gamma_0 + \Delta\Gamma$. This additional damping reflects the efficent exciton-charge carrier scattering. It is assumed to be independent of the time elapsed since excitation. The oscillation amplitude $A(t_D)$ for an excitonic wave packet with propagation time t_{prop} is then given by

$$A(t_D) = A_0\{1 - \exp[-\Delta\Gamma(t_{prop} + t_D)]\}. \quad (8)$$

This expression is valid for $-t_{prop} \leq t_D \leq 0$ and A_0 denotes the relative amplitude of the excitonic polarization wave as compared to the amplitude of the photonic branch. From the time-dependent oscillation amplitude (see inset of Fig. 6) one can therefore derive both propagation time and the value of the pump-induced dephasing. The onset of the oscillation at 1.536 eV corresponds to a transit time of $t_{prop}^{hhX} = 3.8$ ps confirming the effective mass of 0.52 m_0 for hh excitons. Via the delay time dependence recorded slightly above the X
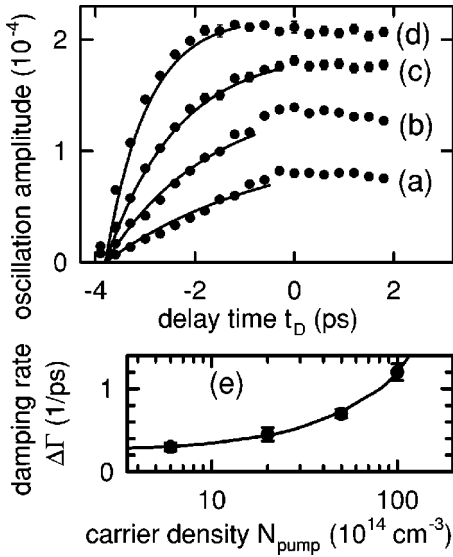
FIG. 7. Amplitude of the spectral oscillations versus delay time extracted at a probe photon energy of 1.533 eV at different excitation densities N_{pump} of 6×10^{14} cm^{-3} (a), 2×10^{15} cm^{-3} (b), 4×10^{15} cm^{-3} (c), and 1×10^{16} cm^{-3} (d). Solid lines: fits according to the theoretical model specified in the text. (e): rate of the pump-induced dephasing versus carrier density N_{pump} extracted from our data. Solid line: fit assuming linear dependence of the scattering rate versus N_{pump}.

+LO threshold at 1.548 eV (see inset of Fig. 6) a propagation time of $t_{prop}^{lhX}=1.7$ ps has been found for lh excitons in agreement with an effective exciton mass of 0.19 m_0.

As displayed in Fig. 7, the delay time-dependent oscillation amplitude is studied as a function of excitation density: for excitation densities N_{pump} below 2×10^{15} cm^{-3} [transients (a) and (b) in Fig. 7] the excitonic polarization is only partially damped by the nonthermal carriers. Raising the density of the pump generated electron-hole plasma to 1×10^{16} cm^{-3}, the layer thickness exceeds the mean free path for the exciton-free carrier scattering and the oscillation amplitude saturates. As may be seen from the transient (d) in Fig. 7, the oscillation amplitude reaches the maximum value significantly before $t_D=0$ corresponding to very fast damping of the excitons. According to Eq. (8), the saturation value determines the splitting ratio of the polarization amplitudes of the polariton branches. For an excess energy of 25 meV the branching ratio is measured to be 2×10^{-4}. This value corresponds to a relative intensity contribution of the excitonic propagation mechanism of the order of 10^{-7} highlighting the extreme sensitivity of the differential method used in our experiments.

As may be seen from Eq. (8), the initial slope of the oscillation amplitude at $t_D=-t_{prop}$ is related to the pump-induced damping $\Delta\Gamma$. The solid lines in Fig. 7 display fits of the delay time-dependent oscillation amplitude according to this model. Figure 7(e) contains the observed values $\Delta\Gamma$ as a function of excitation density N_{pump}.

Our findings suggest a linear dependence $\Gamma=\Gamma_0+\rho N_{pump}$ of the excitonic damping from the density N_{pump} of the generated electron-hole plasma [see the solid line in
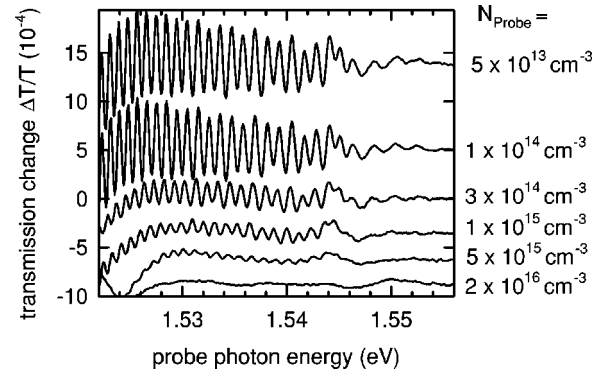

FIG. 8. Differential transmission spectra in the 500 nm specimen for different probe generated carrier densities N_{probe}. The data are recorded 10 ps after injection of a free carrier density of 3×10^{15} cm^{-3} at a lattice temperature of $T_L=20$ K.

Fig. 7(e)]. A coefficient $\rho=9.5\times10^{-5}$ cm^3 s^{-1} is extracted from our results. This value may be compared to the result $\rho=1.6\times10^{-3}$ cm^3 s^{-1} for the fundamental exciton resonance.[29] Apparently, scattering of large-momentum excitons with free carriers is drastically reduced with respect to excitons with wave vector $K\approx0$. The weak scattering for larger kinetic energies may result from the small phase-space overlap of the corresponding excitons and free carriers and from reduced exchange effects.[31]

B. Influence of the probe generated carrier density

In order to observe interferences between different polariton modes, the damping of the excitons has to remain below the critical value Γ_{crit} (see Sec. II). Even if this condition is fulfilled in the unexcited semiconductor layer, one has to consider the interaction of the polaritons employed to detect the propagation beats. The probe pulse that coherently creates large-momentum excitons also generates unbound electron-hole pairs via direct interband transitions. These nonthermal carriers lead to additional dephasing.

Figure 8 shows the experimental results for a varying probe pulse intensity. For carrier densities $N_{probe}\lesssim1\times10^{14}$ cm^{-3} the self-induced dephasing of the probe is negligible. The observed spectra are solely determined by intrinsic properties of the unexcited semiconductor layer. For an increasing carrier density the observed oscillation amplitude decreases. For excitation $N_{probe}\gtrsim1\times10^{16}$ cm^{-3} no beating structure is observed: the excitonic damping is larger than Γ_{crit}.

VI. THEORETICAL DESCRIPTION OF POLARITON PROPAGATION

In this section, we develop a theoretical model based on additional boundary conditions (ABC). Whereas a simple simulation based on Pekar's ABC has been shown to provide a qualitative explanation for a propagation length of 500 nm,[15] we now include all relevant scattering mechanisms calculated in Sec. IV B. A refined model modifying Pekar's ABC is proposed that fits to the observations for all investigated film thicknesses.

A. Additional boundary conditions

As discussed in Sec. II, three exciton polariton modes (P, X_{hh}, X_{lh}, see Fig. 1) are accessible for a given frequency in the absorption continuum of GaAs. Therefore, Maxwell's boundary conditions are not sufficient to determine the branching ratio for these propagating modes at the interface. Additional quantities are necessary to obtain the four unknown parameters, i.e., the amplitude of the reflected electromagnetic wave and of the three transmitted polariton branches.[10]

Until now, rigorous theoretical results for this problem are available only in the frequency regime very close to the fundamental resonance.[13,14] Due to the demanding numerics of microscopic calculations, no results for the amplitude of excitonlike polariton modes in the absorption continuum have been reported. For these continuum states the splitting ratio is only accessible via ABC (for a detailed description, see e.g., Ref. 2). Their appropriate formulation is the subject of extensive theoretical discussions.[11,32–35] All these theories rely on the same basic idea: the dispersion of the exciton polaritons is approximated by the solution of Eq. (1), while phenomenological considerations for the excitonic polarization at the semiconductor surface provide additional conditions for the amplitude of the different polarization waves.

A common formulation of these approaches for the boundaries of a semiconductor layer at $z = \pm d/2$ may be written according to[35]

$$ik_j(1-u)P_j\Big|_{z=\pm l/2} \pm (1+u)\frac{d}{dz}P_j\Big|_{z=\pm l/2} = 0. \quad (9)$$

Here P_j ($j =$ hh,lh) denotes the excitonic polarization and u is the reflection coefficient for excitonic polarization waves at a semiconductor surface. For the case of $u = \pm 1$ Eq. (9) is related to an intuitive physical picture: Pekar's ABC (Ref. 32) with $u = -1$ demand a vanishing excitonic polarization at the semiconductor interface due to the finite real-space volume occupied by a bound electron-hole pair. In contrast, Ting's ABC (Ref. 34) with $u = 1$ assume the flux of excitonic polarization to be zero at the surface. ABC's with differing values of the reflection coefficient u interpolate between Pekar's and Ting's case.

Closely related to these additional boundary conditions is the idea of an exciton-free surface layer. In a slab geometry, this surface layer may be incorporated via a reduced propagation length for the excitonic polarization waves.

To illustrate the consequences of different ABC's on the calculated differential transmission signal, we have simulated the contribution of hh excitons for a 190-nm GaAs specimen. The spectra displayed in Fig. 9 show the change of the sample transmission for two different values of the excitonic damping: The pump pulse is assumed to enhance the homogeneous linewidth from $\Gamma_0 = 0.15$ meV to $\Gamma = 5$ meV. Additional dephasing due to polar optical emission of LO phonons is implemented according to Sec. IV B.

The results may be compared to the experimental findings in the 200-nm specimen [see Fig. 2(b)] taking into account a thin exciton-free surface layer. While Birman's ABC's (Ref. 33) result in a regularly shaped interference pattern [$u = 0$,
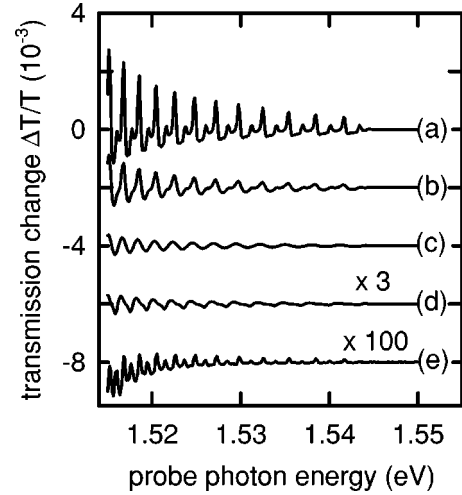

FIG. 9. Differential transmission spectra for the hh polariton contribution calculated with different additional boundary conditions corresponding to varying parameters u for a GaAs layer with 190-nm thickness: (a) Pekar's ABC: $u = -1$, (b) $u = -0.5$, (c) Birman's ABC: $u = 0$, (d) $u = 0.5$. (e) Ting's ABC: $u = 1$.

see Fig. 9(c)], the spectra calculated according to Pekar's ABC (Ref. 32) exhibit larger amplitudes and a substructure [$u = -1$, see Fig. 9(a)]. Assuming reflection of excitonic polarization waves without phase jump [$u = 1$, Ting's ABC (Ref. 34)] results in oscillation amplitudes much too small to explain our experimental findings (see e.g. Fig. 2). Interestingly, this finding is consistent with a recent study of the linear optical properties of thin films of GaAs given by Schneider *et al.*[14] They have found Pekar's ABC to fit better to their result for the absorption coefficient as compared to other formulations of ABC although deviations from a microscopic treatment are significant near the fundamental resonance.

The decreasing oscillation amplitude for higher photon energies reflects the smaller photonic contribution of the hh exciton polaritons (see Sec. II) and the weaker excitation of this branch: a sharp semiconductor interface may, in principle, provide arbitrary momentum changes **K**. However, the corresponding Fourier components in momentum space decrease with $1/K$ and the splitting ratio for the excitonic polarization is therefore reduced for larger transition energies. The discontinuity of the spectra one LO phonon energy above the exciton is explained by the onset of polar optical scattering discussed in Sec. IV B.

B. Simulation of experimental spectra

Based on the theory described in the preceding section detailed simulations have been performed to analyze the experimental results for the different layer thicknesses. The dielectric layers surrounding the investigated specimen (AlGaAs cladding, antireflection coating, and sapphire substrate) are included in a transfer matrix formalism. In all theoretical spectra, we have calculated the difference of the absorption of the GaAs layer for different values of the polaritonic damping corresponding to pump-induced modifications of the dephasing times of the excitons.
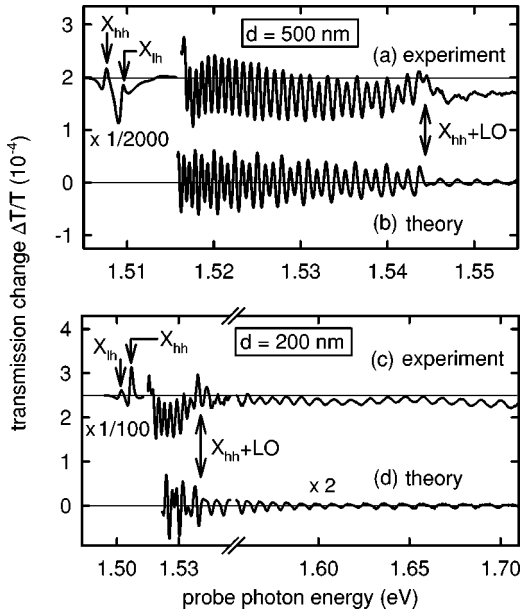
FIG. 10. Spectrally resolved transmission changes recorded 10 ps after injection of free electron-hole pairs in GaAs layers of a thickness of 500 nm (a) and 200 nm (c) at a temperature of $T_L = 20$ K. The pump generated carrier density is 3×10^{15} cm^{-3} and 5×10^{15} cm^{-3}, respectively. Theoretical simulations with parameters specified in the text are displayed in the spectra (b) and (d).

In our calculation, we only consider transmission changes due to the dephasing of $1s$ hh and lh excitons. The influence of higher bound excitonic states and the damping of the photonlike branch by pump generated carriers is neglected (for a discussion of the influence of the excitonic continuum, see Ref. 36). The dispersion relation of the three polariton branches is taken from the calculations of Sec. II. Scattering with optical and acoustic phonons is implemented according to the theory in Sec. IV.

The results for the 500-nm specimen are displayed in Fig. 10(b). The background damping is assumed to be 0.2 meV and 0.6 meV for hh and lh excitons independent from their kinetic energy. The damping of the large-momentum excitons with the pump injected electron-hole plasma is estimated to be 0.6 meV and 0.5 meV for the hh and lh branch, respectively. The simulation reproduces the experimental findings [see Fig. 10(a)] quantitatively over a large spectral region including the beating of the hh and lh contributions near $X + LO$. From the shape of the oscillations the reflection coefficient for excitonic polarization waves is determined to be $u = -0.5$. Taking into account the spectral resolution of 0.6 meV in the experiment, good agreement with the experimental finding is obtained in the range $-1 \leq u \leq -0.5$: a possible substructure reminiscent of the spectrum in Fig. 9 (a) is not resolvable in the 500-nm specimen.

Both experimental and theoretical results obtained in a 200-nm GaAs sample are depicted in Figs. 10(c) and 10(d). A background damping of 0.6 meV is assumed for both exciton branches. The damping due to pump-induced exciton-free carrier scattering is set to 0.7 meV and 1.0 meV for hh and lh excitons, respectively. The best agreement with experiment is found with a reflection coefficient $u = -0.4$. The
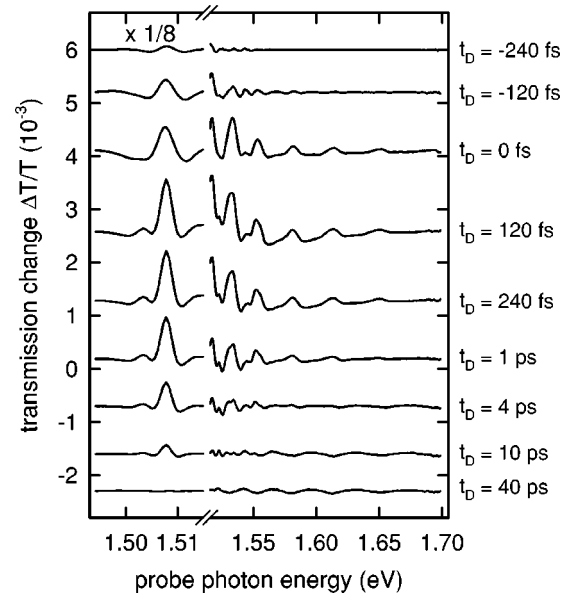

FIG. 11. Differential transmission spectra recorded in the 50-nm specimen for various delay times t_D. The pump pulse excites an electron-hole plasma with pair density 3×10^{16} cm^{-3}.

underestimation of the oscillation amplitude with respect to the experimental observations may be a first hint towards deviations from a theory based on ABC: the calculated splitting ratio for lh excitonlike polaritons is too small to reproduce the observed propagation beats for large transition energies. For probe photon energies above 1.6 eV the simulation results in larger oscillation periods as compared to the experiment. This effect is a consequence of the nonparabolicity of the lh exciton dispersion.

VII. DISCUSSION OF THE RESULTS FOR THE 50-nm LAYER: INTERFACE EFFECTS

Further insight into polariton effects and the microscopic electrodynamics near semiconductor interfaces is obtained investigating differential transmission spectra of a 50-nm film of GaAs. Femtosecond transition times of excitonic wave packets open up the possibility to study dephasing of large-momentum excitons by carrier distributions far from a thermal distribution. For the first time, a film thickness comparable to the excitonic Bohr radius is investigated systematically. As a consequence, surface properties begin to dominate the experimental results. This regime opens up the possibility to study the nonlinear optics of semiconductor interfaces and to gain new information on the excitonic polarizability near the surface.

Figure 11 shows polariton interference spectra for different delay times t_D after generation of unbound electron-hole pairs with a 100-fs pump pulse centered at 1.54 eV. The propagation beats are observable up to transition energies as large as 1.7 eV: the relaxation of hh excitons via polar optical emission of LO phonons is no longer sufficient to damp out the excitonic polarization above the $X + LO$ threshold. As discussed below, no contributions of lh excitons are observed and the signal is dominated by the hh exciton polaritons.

Upon closer inspection of the observations for negative delay times (see Sec. V A), a propagation time of 250 fs is found for hh excitons with a kinetic energy of 25 meV, consistent with an effective propagation length of 30 nm. This value is a direct hint for an exciton-free surface layer extending approximately one Bohr radius of $a_B = 11.5$ nm from both interfaces. New as compared to the observations in the 200-nm and 500-nm specimens is a substructure of the oscillations reminiscent of the theoretical simulations with Pekar's ABC in Sec. VI A [see Fig. 9(a)].

As shown in Ref. 37, this feature is incorporated in the ABC approach presented in Sec. VI A. To get a more intuitive picture of this substructure, the same phenomenon may also be discussed as a consequence of the quantized center-of-mass motion of excitons in thin samples.[5,37-40] The wave vector K_z of an exciton in a layer with thickness d is restricted to $K_z = \pi n / d$ with an integer n. For dipole transitions of excitons with odd or even n, different parity selection rules have been found[41] leading to different amplitudes for these excitons in the observed spectra.

At $t_D = 1$ ps in Fig. 11 the observed polariton beating has significantly decreased with respect to the observations for earlier positive delay times. This finding clearly demonstrates that the relaxation of the pump generated nonequilibrium carriers into a quasithermal distribution drastically reduces the damping of the large-momentum excitons. For delay times of a few picoseconds the amplitude of both the bleaching of the exciton resonance and the oscillating structure decreases. Interestingly, the phase of the beating structure in the absorption continuum depends on the delay time. This is a new feature absent for thicker specimens and cannot solely result from modifications of the excitonic damping. Via screening of the Coulomb interaction also the Bohr radius a_B of the exciton is enlarged: therefore, changes in the thickness of the exciton-free surface layer contribute to the differential transmission signals.

To theoretically analyze the observations, numerical simulations have been performed including an energy-dependent dead layer on both semiconductor surfaces. Only hh excitons have been included for this layer thickness. Calculations for the signal contributions of lh excitons predict only very small transmission changes for the following reasons: (i) as may also be seen from the results below $X + LO$ for thicker specimens, the amplitude of the lh beating structure is weak as compared to the hh oscillations due to the smaller oscillator strength of lh excitons; (ii) the effective propagation length of lh exciton polaritons in a 50-nm layer is expected to be extremely short due to their larger Bohr radius.

Figure 12 shows the transmission changes calculated for the 50-nm layer. For a delay time of $t_D = 1$ ps the excitonic wave packet is efficiently damped by the pump generated electron-hole plasma. The theoretical curve in Fig. 12(b) is obtained with a background damping of 0.3 meV and a dephasing of 4 meV due to exciton-free carrier scattering. The shape of the oscillating structure is used to determine a reflection coefficient of $u = -0.5$. To reproduce the observed peak positions over a large energetic range, an energy-dependent exciton-free surface layer is assumed (see inset of Fig. 12): for low kinetic energies the thickness of the dead
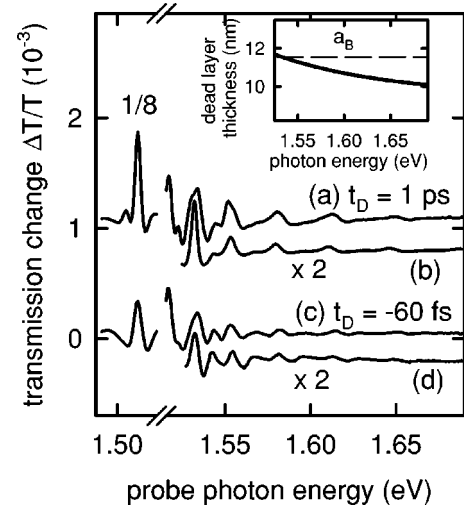

FIG. 12. Differential transmission spectra in the 50-nm layer: (a) and (c) as recorded at the delay time $t_D = 1$ ps and $t_D = -60$ fs, respectively. (b) Theoretical simulation for dominant pump-induced damping. (d) Calculation assuming a pump-induced modification of the exciton-free dead layer. Inset: energy-dependent dead layer used for the calculation. The dashed line indicates the Bohr radius a_B of hh excitons in GaAs.

layer is found to coincide with the excitonic Bohr radius a_B, while it decreases slightly for large kinetic energies. Except for an underestimate of the absolute value of the transmission changes, a good overall agreement with the experimental findings Fig. 12(a) is achieved.

For the case of a slightly negative delay time $t_D = -60$ fs a different situation is found: due to the short transit times of the polaritonic wave packet, the differential transmission is more sensitive to surface effects as compared to the damping of the excitons: injecting free carriers at the end of the polariton propagation through the layer, the excitons do not suffer efficient damping. However, ultrafast changes of the properties of the exit surface modify the reconversion of the excitonlike polaritons to photons. Especially, the electron-hole interaction is partially screened by the pump-induced carriers and the dead layer may be enlarged. Moreover, the surface potential and small built-in electric fields near the second interface may be modified.[42] As a consequence, the effective propagation length for exciton polaritons is reduced. Figure 12(d) shows the transmission changes calculated for a pump-induced increase of the dead layer by 3 nm. The agreement with the experimental findings Fig. 12(c) supports the interpretation as ultrafast modification of the exciton-free surface layer predicted in Ref. 43.

It should be noted that the interference spectrum of the 50-nm specimen may also be interpreted assuming an energy-independent dead layer and a nonparabolic hh band. However, this model requires an unexpectedly strong variation of the effective hh mass to reproduce the peak positions over a broad spectral range.

VIII. SUMMARY

In conclusion, a powerful technique giving direct spectroscopic access to the properties of large momentum excitons

in GaAs has been developed. We want to point out that the method is quite general and applicable to various questions concerning excitonic effects and spatial dispersion in crystalline solids. For the first time, excitonic dispersion relations are studied up to 300 meV above the band edge providing detailed information about the interaction dynamics of bound electron-hole states with large kinetic energies. A striking difference of the Fröhlich coupling for the exciton branches is found: lh excitons consisting of quasiparticles with similar effective masses, are surprisingly robust against polar optical interaction. This effect may be ascribed to a destructive interference in the corresponding scattering matrix element. The femtosecond time resolution of our experimental technique provides direct access to the scattering of highly energetic excitons with nonthermal carrier distributions. Interestingly, the scattering of large-momentum excitons with free carriers is found to be much less efficient as for the case of excitons with negligible center-of-mass motion.

The findings for different layer thicknesses elucidate the long-standing problem of polariton propagation in thin semiconductor slabs. For layer thicknesses large as compared to the excitonic Bohr radius a theoretical model slightly modifying Pekar's additional boundary conditions is found to explain the experimental results. For small propagation lengths the results are very sensitive to microscopic properties of the polarizability near semiconductor interfaces. We propose a phenomenological model including an energy-dependent exciton-free dead layer at the surface reproducing the observed spectra. A full microscopic understanding of our results will require a simultaneous solution of Schrödinger's and Maxwell's equations at the semiconductor interface.

[1] J. Shah, *Ultrafast Spectroscopy of Semiconductors and Semiconductor Nanostructures* 2nd ed. (Springer-Verlag, Berlin 1999).

[2] *Proceedings of the International Meeting on Excitons in Confined Systems*, *Rome, 1987*, edited by R. Del Sole, A. D'Andrea, and A. Lapiccirella (Springer, Berlin, 1988); M. Ueta, H. Kanzaki, K. Kobayashi, Y. Toyozawa, and E. Hanamura, *Excitonic Processes in Semiconductors* (Springer, Berlin, 1986).

[3] J. J. Hopfield, Phys. Rev. **112**, 1555 (1958).

[4] V. A. Kiselev, B. S. Razbirin, and I. N. Uraltsev, Phys. Status Solidi B **72**, 161 (1975).

[5] A. Tredicucci, Y. Chen, F. Bassani, J. Massies, C. Deparis, and G. Neu, Phys. Rev. B **47**, 10 348 (1993).

[6] A. C. Schäfer and D. G. Steel, Phys. Rev. Lett. **79**, 4870 (1997).

[7] D. Fröhlich, A. Kulik, B. Uebbing, A. Mysyrowicz, V. Langer, H. Stolz, and W. van der Osten, Phys. Rev. Lett. **67**, 2343 (1991).

[8] J. S. Nägerl, B. Stabenau, G. Böhne, S. Dreher, R. G. Ulbrich, G. Manzke, and K. Henneberger, Phys. Rev. B **63**, 235202 (2001).

[9] S. Nüsse, P. Haring Bolivar, H. Kurz, F. Levy, A. Chevy, and O. Lang, Phys. Rev. B **55**, 4620 (1997).

[10] S. I. Pekar, Zh. Eksp. Teor. Fiz. **34**, 1176 (1958) [Sov. Phys. JETP **7**, 813 (1958)].

[11] K. Henneberger, Phys. Rev. Lett. **80**, 2889 (1998).

[12] A. Stahl, Phys. Status Solidi B **106**, 575 (1981).

[13] J. Tignon, T. Hasche, D. S. Chemla, H. C. Schneider, F. Jahnke, and S. W. Koch, Phys. Rev. Lett. **84**, 3382 (2000).

[14] H. C. Schneider, F. Jahnke, S. W. Koch, J. Tignon, T. Hasche, and D. S. Chemla, Phys. Rev. B **63**, 045202 (2001).

[15] G. Göger, M. Betz, A. Leitenstorfer, M. Bichler, W. Wegscheider, and G. Abstreiter, Phys. Rev. Lett. **84**, 5812 (2000).

[16] A. Leitenstorfer, C. Fürst, A. Lauberau, W. Kaiser, G. Tränkle, and G. Weimann, Phys. Rev. Lett. **76**, 1545 (1996).

[17] M. Betz, G. Göger, A. Leitenstorfer, K. Ortner, C. R. Becker, G. Böhm, and A. Lauberau, Phys. Rev. B **60**, R11 265 (1999).

[18] M. Combescot and O. Betbeder-Matibet, Solid State Commun. **80**, 1011 (1991).

[19] G. Fishman, Solid State Commun. **27**, 1097 (1977).

[20] M. Matsushita, J. Wicksted, and H. Z. Cummins, Phys. Rev. B **29**, 3362 (1984).

[21] C. Fürst, A. Leitenstorfer, and A. Lauberau, IEEE J. Sel. Top. Quantum Electron. **2**, 473 (1996).

[22] M. S. Skolnick, A. K. Jain, R. A. Stradling, J. Leotin, J. C. Ousett, and S. Askenazy, J. Phys. C **9**, 2809 (1976).

[23] T. Ruf and M. Cardona, Phys. Rev. B **41**, 10 747 (1990).

[24] Y. Toyozawa, Prog. Theor. Phys. **12**, 111 (1959).

[25] C. Fürst, A. Leitenstorfer, A. Lauberau, and R. Zimmermann, Phys. Rev. Lett. **78**, 3733 (1997).

[26] B. K. Ridley, *Quantum Processes in Semiconductors* (Clarendon Press, Oxford, 1993).

[27] R. Scholz, J. Appl. Phys. **77**, 3219 (1995).

[28] T. Brudevoll, T. A. Fieldly, J. Baek, and M. S. Shur, J. Appl. Phys. **67**, 7373 (1990).

[29] L. Schultheis, J. Kuhl, A. Honold, and C. W. Tu, Phys. Rev. Lett. **57**, 1635 (1986).

[30] J. Lee, E. S. Koteles, and M. O. Vassell, Phys. Rev. B **33**, 5512 (1986).

[31] S. Schmitt-Rink, D. S. Chemla, and D. A. B. Miller, Phys. Rev. B **32**, 6601 (1985).

[32] S. I. Pekar, Zh. Eksp. Teor. Fiz. **33**, 1022 (1957) [Sov. Phys. JETP **6**, 785 (1958)].

[33] J. L. Birman and J. J. Sein, Phys. Rev. B **6**, 2482 (1975).

[34] C. S. Ting, M. J. Franckel, and J. L. Birman, Solid State Commun. **17**, 1285 (1975).

[35] P. Halevi and R. Fuchs, J. Phys. C **17**, 3869 (1984).

[36] E. Muljarov and R. Zimmermann, in *Proceedings of the 25th International Conference on the Physics of Semiconductors, Osaka, 2000*, edited by N. Miura and T. Ando (Springer, Berlin, 2001), pp. 101–102.

[37] V. A. Kiselev, I. V. Makarenko, B. S. Razbirin, and I. N. Uraltsev, Fiz. Tverd. Tela **19**, 2348 (1977) [Sov. Phys. Solid State **19**, 1374 (1977)].

[38] V. A. Kiselev, I. N. Uraltsev, and I. V. Makarenko, Solid State Commun. **53**, 591 (1985).

[39] S. Adachi, S. Takeyama, Y. Takagi, J. J. Dubowski, and E. Deleporte, Superlattices Microstruct. **16**, 1 (1994).

[40] P. Lefebvre, V. Gallo, N. Magnea, T. Taliercio, J. Allegre, and H. Mathieu, Phys. Rev. B **56**, R10 040 (1997).

[41] H. Tuffigo, R. T. Cox, N. Magnea, Y. Merle d'Aubigne, and A.

Millon, Phys. Rev. B **37**, 4310 (1988).

[42] S. Jaziri and R. Bennaceur, in *Excitons in Confined Systems*, edited by R. Del Sole, A. D'Andrea, and A. Lapiccirella (Springer-Verlag, Berlin, 1988).

[43] S. Bischoff, A. Knorr, and S. W. Koch, Phys. Rev. B **55**, 7715 (1997).